

1 | METHODS

1.1 HI-C DATA

1.1.1 Mapping

Raw Hi-C reads were downloaded from published datasets (Table 1) through the Gene Expression Omnibus (GEO)^[1] or the Short Read Archive (SRA)^[2] with identifiers: GSE35156 (H1 hESC), GSE18199 (K562) and SRX030113 (GM12878). These paired reads were mapped independently to a reference genome: hg19/GRCh37 for human data, and mm10/GRCm38 for mouse.

Mapping was performed using the hiclib software package^[6] and bowtie2^[7] with the `--very-sensitive` flag. An iterative mapping approach was used to maximise the number of aligning fragments.^[6] Each fragment end was aligned first using short terminal sub-sequences. Those unmapped or with ambiguous mapping were then taken forward into the next iteration and extended until the entire fragment end had been aligned. Those remaining pairs with one or more unmapped ends were discarded.

1.1.2 Filtering

After mapping, interactions are first aggregated into restriction fragments then by regular binning of various resolutions (particularly 40 kb, 100 kb and 1 Mb). Several filters were applied at this stage, with the following cases removed:^[6]

- Reads directly adjacent to a restriction enzyme site (within 5 bp)
- Identical read pairs (presumed PCR duplicates)
- Very large restriction fragments (> 100 kb) which are likely from a repetitive or poorly-assembled region
- Extremely over-represented fragments (top .05%) which may throw-off eigenvector derivation

1.1.3 Correction

Iterative correction and eigenvector expansion (ICE) is an approach to normalisation and processing Hi-C data, implemented as software library written in python.^[6] The iterative correction algorithm performs matrix balancing with the aim of generating a doubly stochastic matrix from raw interaction counts. That is, such that symmetric matrix A has both row and columns of equal sum. In practice, this effectively enforces "equal visibility" of each fragment, correcting for previously-described biases in interaction recovery such as GC-content and fragment length^[8] but without explicitly modelling

Table 1: Public Hi-C data used in this work.

Cell line	Total reads	Accession	Citation
Gm12878	31×10^6	SRX030113	3
H1 hESC	331×10^6	GSE35156	4
K562	36×10^6	GSE18199	5
Cortex	373×10^6	GSE35156	4
mESC	476×10^6	GSE35156	4
IMR90	355×10^6	GSE35156	4

these latent variables. This procedure is thus converting actual interaction counts into normalised interaction frequencies (IF), and to relative rather than absolute quantities. Scaling of IFs permits comparison of Hi-C experiments with very different sequencing depths (as is the case in this work, see Table 1). Despite differences in the levels of sequencing, otherwise the experiment methods underlying the produced Hi-C data were similar: the HindIII restriction enzyme was used in each case and the Hi-C protocol was largely unchanged (that is, we did not consider data from Hi-C variants such as TCC^[3] and *in-situ* Hi-C^[9]).

1.1.4 Eigenvector calculation

Additional functionality provided by ICE is the eigenvector expansion of normalised contact maps. Eigenvectors from observed/expected matrices were chosen for consistency with Lieberman Aiden *et al.*,^[5] as opposed to the related eigenvectors calculated in Imakaev *et al.*^[6] from the corrected maps alone. The details of this procedure are described in section 1.5.2. Briefly, observed contacts (O) are divided by an expected matrix (E) which is generated by averaging the super- and sub-diagonals of the O matrix. That is, the E matrix gives the expected value of interactions at a given distance.

Importantly, the first two principle components (PCs) were calculated, and that with the highest absolute Spearman correlation with GC content is taken to reflect A/B compartmentalisation. PC eigenvectors were then orientated to positively correlate with GC, ensuring positive values reflected A compartments and negative values B compartments. Another subtlety is the calculation of eigenvectors per chromosome arm as opposed to per chromosome, this prevents issues with some meta- and submetacentric chromosomes where the first principle component indicated chromosome arms.^[5,6] Eigenvector expansion was performed on both 1 Mb and 100 kb matrices, below these resolutions results became less stable, and it has been shown that eigenvectors at

1.2 ENCODE FEATURES

Genome-wide ChIP-seq datasets for: 22 DNA binding proteins and 10 histone marks were made available by the ENCODE consortium^[10,11] along with DNase I hypersensitivity and H2A.z occupancy, for each of the Tier 1 ENCODE cell lines used in this work: H1 hESC, K562 and GM12878. These data were pre-processed using MACSv2^[12] to produce fold-change relative to input chromatin. GC content was also calculated and used in the featureset to give 35 total inputs (Table 2).

Table 2: ChIP-seq and other public datasets used in this work.

Histone modifications	DNA binding proteins	Other
H3K27ac, H3K27me3, H3K36me3, H3K4me1, H3K4me2, H3K4me3, H3K79me2, H3K9ac, H3K9me3, H4K20me1	ATF3, CEBPB, CHD1, CHD2, CMYC, CTCF, EGR1, EZH2, GABP, JUND, MAX, MXI1, NRSF, POL2, P300, RAD21, SIX5, SP1, TAF1, TBP, YY1, ZNF143	DNase, GC content, H2A.Z

1.2.1 Clustering input features

To quantify collinearity of input features, correlation matrices built from genome-wide vectors of input feature measures were build and hierarchically

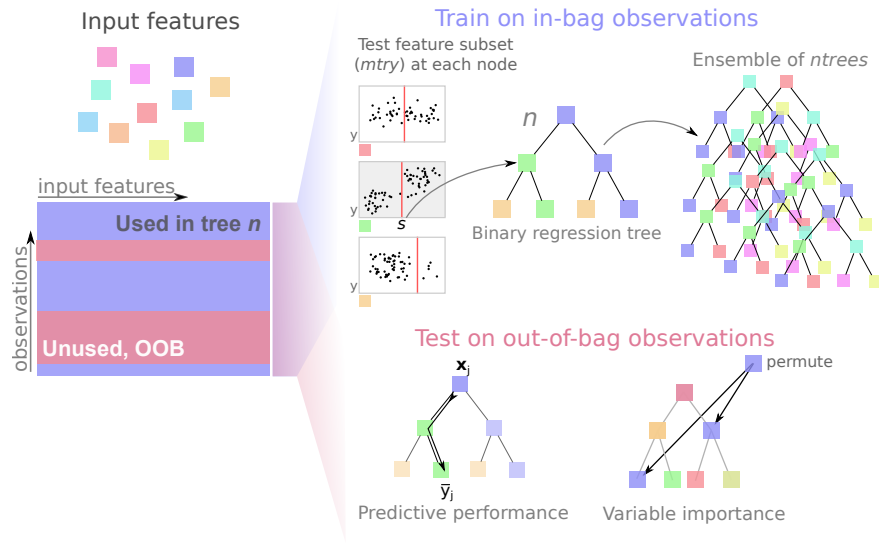


Figure 1: Random Forests overview. Random Forests are an ensemble of bagged, de-correlated classification or regression trees first described by Breiman.^[14]

clustered. The “significance” of observed clustering was assessed using sub- and super-sampled bootstrapping, with stable clusters deemed significant, as implemented in the pvc1ust R package.^[13]

1.3 MODELLING

1.3.1 Random Forest

Random Forest (RF) regression,^[14] was used as implemented in the R package randomForest.^[15] The RF algorithm (Fig. 1) makes use of a collective of regression trees (size *ntrees*), each built from a bootstrapped sample of the training set. In growing each tree, a small number of variables (*mtry*) is tested at each bifurcation node, and that which minimises the variance in child node subsets is selected at a specific threshold. Having trained a group of trees, these can then be used as predictive tools by inputting a vector of features to each tree and averaging the output leaf node value across the forest. RF regression was used as it is known to be one of the most powerful regression methods developed to date,^[16,17] typically providing low bias and low variance predictions without the need for variable selection.^[18,19]

Additionally the RF method represents an example of “algorithmic modelling”^[20] in that it makes no assumptions about the underlying data model. Parameters of $mtry = \frac{n}{3}$ (where *n* is the number of input features) and *ntrees* = 200 were assumed as they are known to be largely insensitive;^[19,21] this was verified with the dataset used in this work (Fig. 2).

Variable importance within Random Forest regression models was measured using mean decrease in accuracy in the out-of-bag (OOB) sample. This represents the average difference (over the forest) between the accuracy of a tree with permuted and unpermuted versions of a given variable (Fig. 1), in units of mean squared error (MSE).^[17,19]

1.3.2 Model performance

The effectiveness of the modelling approach was measured by four different metrics. Prediction accuracy was assessed by the Pearson correlation coefficient between the OOB predictions and observed eigenvectors, and the root mean-squared error (RMSE) of the same data. Classification error,

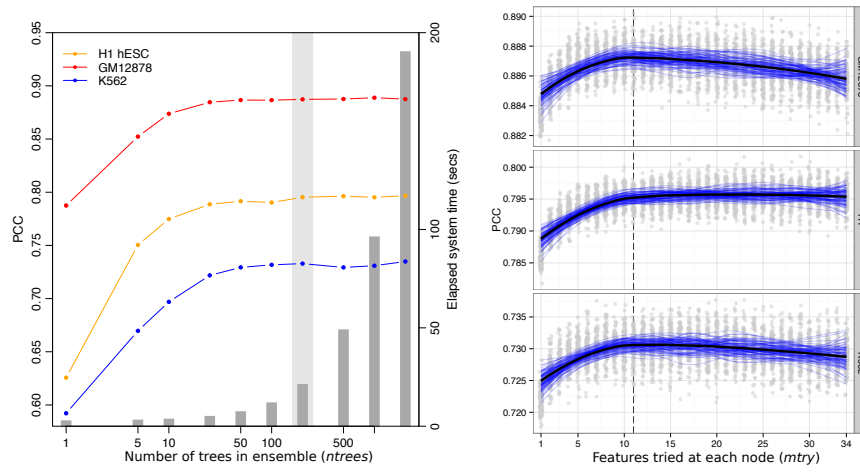


Figure 2: Confirmatory Random Forest parameter optimisation. Two user-facing Random Forest parameters are known to be insensitive over a broad range.^[21] Optimisations for *ntrees* (the number of trees in the forests) and *mtry* (the number of features tested at each node) are shown for three different models, with typical values of 200 trees and $\frac{1}{3}$ of input variables highlighted.

when predictions were thresholded into $A \geq 0; B < 0$, was also calculated using accuracy (% correct classifications or True Positives) and area under the receiver operating characteristic (AUROC) curve. Together these give a comprehensive overview of the model performance, both in terms of regression accuracy of the continuous eigenvector, and in how that same model could be used to label discrete chromatin compartments.

For cross-application of cell type specific models, a single Random Forest regression model was learned from all 1 Mb bins for a given cell type. This was then used to predict all bins from each of the other two cell types.

To test the sensitivity of the models to resolution, we also applied cell-type specific models learnt at 1 Mb resolution to input features binned at 100 kb.

1.3.3 Other modelling approaches

Linear regression was used as a baseline for comparison with more complicated approaches such as Random Forest. If the same modelling accuracy could be achieved with simple multiple linear regression, this would be a faster and more interpretable modelling framework.

Partial least squares (PLS) regression was also used to model compartment profiles. PLS regression is well-suited to highly correlated inputs, employing a dimensionality reduction step to help address this redundancy, yet lacks the interpretability of a multiple linear regression. Similar to RF, PLS regression is aimed at building highly-predictive models rather than understanding singular relationships between a predictor and independent variable.^[22] The `plsdepot` R implementation of PLS regression was used in this work.

1.3.4 Graphical lasso

Regularised models made use of the Graphical LASSO^[23] (least absolute shrinkage and selection operator) as a method of L_1 -norm based regularisation, implemented via the `glasso` R package. The graphical lasso provides tuneable regularisation which is capable of feature selection via minimising regression parameters to 0. It was chosen in this case due to the multi-

collinearity of the featureset, the algorithm's fast speed of execution and the intuitiveness a graphical model presents.^[23]

More specifically, the graphical lasso regulates the number of os in the inverse covariance matrix, $\Theta = \Sigma^{-1}$, also known as the precision matrix. Then if element $\theta_{ij} = 0$, the variables X_i and X_j can be said to be conditionally independent, given the remaining variables.^[24] The algorithm minimises a negative log-likelihood (Eqn. 1^[24]) given the tuning parameter λ , which was tuned in this case to leave a small number of variables (< 10) directly dependent on the eigenvector data.

$$\underset{\Theta \succ 0}{\text{minimise}} f(\Theta) := -\log \det(\Theta) + \text{tr}(\mathbf{S}\Theta) + \lambda \|\Theta\|_1 \quad (1)$$

1.4 VARIABLE REGIONS

1.4.1 Stratification by variability

Median absolute deviation (MAD) was chosen as a robust measure of the variability in a given 1 Mb block between the three primary cell types used in this work: H1, K562 and GM12878. Blocks were ranked by this measure and split into thirds that represented "low" variability (the third of blocks with the lowest MAD), "mid" and "high" variability. Each subgroup was then independently modelled using the previously-described Random Forest approach.

"Flipped" regions are those whose compartment state differs in one cell type relative to the other two. For example, if a 1 Mb bin was classified as "open" in H1 hESC and "closed" in both K562 and GM12878, this is said to be a "flipped" compartment (to open).

1.4.2 Enhancer enrichment

Chromatin state annotations used in this work were retrieved from the ChromHMM^[25] and SegWay^[26] combined annotations.^[27] These represent the consensus from two independent chromatin state prediction algorithms, and ignore regions of apparent disagreement; hence in theory making more robust and conservative predictions than either algorithm independently. Nevertheless, Hoffman *et al.* caution that in areas of disagreement, each algorithm may highlight differing biological phenomena so should also be considered separately.^[27]

The set of state predictions from the combined algorithms are:

1. Predicted transcription start sites (TSS)
2. Promoter flanking regions
3. Transcribed regions
4. Repressed regions
5. Predicted enhancers
6. Predicted weak enhancer or *cis* regulatory element
7. CTCF-enriched elements

Short, discrete state predictions such as enhancers were considered "shared" if there was an overlapping enhancer annotation in either of the two other cell types, and labelled as "tissue-specific" otherwise. This was repeated for each of the called chromatin states.

1.5 BOUNDARIES

1.5.1 TADs

TAD boundaries were called using the software provided in Dixon *et al.*^[4] using their recommended parameters. For the generation of boundary profiles, input features were averaged into 40 kb bins spanning ± 450 kb from the boundary bin.

To test for the enrichment or depletion of a chromatin feature over a given boundary, a two tailed Mann-Whitney test was used to compare the boundary bin with the ten outermost bins of the window (5 from either side). The significance level at $\alpha = 0.01$ was then Bonferonni-adjusted for multiple testing correction, and results with p -values exceeding this threshold were deemed significantly enriched or depleted at a given boundary.

To compare boundaries between cells, each TAD boundary called in K562 and GM12878 were compared with those called in H1 hESC. For each boundary, the minimum absolute difference to the nearest matching boundary in H1 hESC was recorded, and this was then compared with a null model of an equal number of boundaries randomly-placed along available bins. A Kolmogorov-Smirnov test was then used to compare the empirical cumulative distributions of these distances.

1.5.2 Compartments

Eigenvectors were calculated as described in section 1.1.4. A/B compartmentalisation has previously been called simply from the properly-orientated principle component eigenvector, with positive values representing a bin in an A compartment state, and negative values representing a bin in a B, more repressive state.^[5]

Compartment boundaries were called by first training a two-state hidden Markov model (HMM) on the compartment eigenvector and then using the Viterbi algorithm to predict the most likely state sequence that produced the observed values. The point at which transitions occurred between states was taken as a boundary which was then extended ± 1.5 Mb to give a 3 Mb window in which a boundary was thought to occur.

Boundary enrichments and alignments were tested in the same manner as TADs, described in section 1.5.1.

1.5.3 MetaTADs

MetaTADs are a concept discovered by collaborators. Their method for calling such features involve the constrained hierarchical clustering of neighbouring TADs with the greatest inter-TAD contacts. This results in a tree of increasing metaTAD aggregation. For boundary analysis of metaTADs, again a similar approach was used to that of TADs (section 1.5.1) but thresholded to within a given range of sizes. MetaTADs below 10 Mb were excluded, as to have no lower bound results in $\frac{2}{3}$ of all TAD boundaries likewise considered MetaTAD boundaries, reducing the power to analyse any differences. 10 Mb was chosen in an attempt to compromise minimising the overlap between TAD and metaTAD boundaries, while also retaining a large enough sample size. An upper bound of 40 Mb was also chosen, as beyond this threshold inter-TAD contacts were found to be no higher than expected by chance. In practice, the tree-like structure means any upper-bound has little impact as a filter: in almost all cases, any boundary in a metaTAD of size > 40 Mb will also form metaTADs below this value. Additionally, the hierarchical nature of metaTADs means that some boundaries are present at multiple levels of the tree. Only one case of each boundary position was tested for feature enrichments.

1.6 GIEMSA BAND COMPARISON

Cytogenic band data and Giemsa stain results were downloaded from the UCSC genome browser (table cytoBandIdeo). The genomic co-ordinates are an approximation of cytogenic band data inferred from a large number of FISH experiments.^[28]

To compare G-band boundaries with our compartment data, we allowed for a ± 500 kb inaccuracy in G-band boundary. For each G-band boundary, the minimum absolute distance to any compartment or TAD boundary was calculated for each cell type. To generate a null model, ...

1.7 NUCLEAR POSITIONING

Previously published data on chromosome positioning preference within the nucleus was used to label each chromosome as “inner”, “middle” or “outer”.^[29] Chromosomes whose DAPI hybridisation signals were significantly enriched ($p \leq 2 \times 10^{-2}$) in the inner nuclear shell, as defined by Boyle *et al.*^[29], made up the “inner” group and included chromosomes 1 and 16. Similarly the “outer” group had enriched signals ($p \leq 5 \times 10^{-3}$) in the outer shell relative to the inner nuclear shell and included chromosomes 2, 3, 11-13 and 18. The remaining chromosomes in our filtered dataset, 6, 14 and 15, were assigned to the “middle” group and showed no significant to either inner or outer nuclear shells ($p \geq 0.1$).^[29] The significance of the difference in distribution of eigenvectors in the inner versus outer shell was determined by a one-sided Kolmogorov-Smirnov (K-S) test, with the alternative hypothesis that the empirical cumulative density function of the inner chromosome eigenvectors F_{inner} is greater-than or equal-to F_{outer} . This chromosomal positioning data was measured in lymphoblastoid cells though nuclear architecture is thought to be largely conserved between cell types^[30,31] and even higher primates.^[32]

1.8 GENE ONTOLOGY ANALYSIS

Variable regions (section 1.4.1) were tested for functional enrichments using Gene Ontology (GO) annotations.^[33] The DAVID tool^[34] was used to compare GO terms for genes located in variable compartments with a background set of genes within all annotated compartments.

REFERENCES

- [1] Barrett T, Wilhite SE, Ledoux P, Evangelista C, Kim IF, Tomashevsky M, Marshall Ka, Phillippy KH, Sherman PM, *et al.* (2013) NCBI GEO: archive for functional genomics data sets—update. *Nucleic acids research*, **41**(Database issue): D991–5.
- [2] Leinonen R, Sugawara H, Shumway M (2011) The sequence read archive. *Nucleic acids research*, **39**(Database issue): D19–21.
- [3] Kalhor R, Tjong H, Jayathilaka N, Alber F, Chen L (2012) Genome architectures revealed by tethered chromosome conformation capture and population-based modeling. *Nature biotechnology*, **30**(1): 90–8.
- [4] Dixon JR, Selvaraj S, Yue F, Kim A, Li Y, Shen Y, Hu M, Liu JS, Ren B (2012) Topological domains in mammalian genomes identified by analysis of chromatin interactions. *Nature*, **485**(7398): 376–80.
- [5] Lieberman-Aiden E, van Berkum NL, Williams L, Imakaev M, Ragoczy T, Telling A, Amit I, Lajoie BR, Sabo PJ, *et al.* (2009) Comprehensive mapping of long-range interactions reveals folding principles of the human genome. *Science*, **326**(5950): 289–93.
- [6] Imakaev M, Fudenberg G, McCord RP, Naumova N, Goloborodko A, Lajoie BR, Dekker J, Mirny LA (2012) Iterative correction of Hi-C data reveals hallmarks of chromosome organization. *Nature methods*, **9**(10): 999–1003.
- [7] Langmead B, Salzberg SL (2012) Fast gapped-read alignment with Bowtie 2. *Nature methods*, **9**(4): 357–9.
- [8] Yaffe E, Tanay A (2011) Probabilistic modeling of Hi-C contact maps eliminates systematic biases to characterize global chromosomal architecture. *Nature genetics*, **43**(11): 1059–65.
- [9] Rao S, Huntley M, Durand N, Stamenova E, Bochkov I, Robinson J, Sanborn A, Machol I, Omer A, *et al.* (2014) A 3D Map of the Human Genome at Kilobase Resolution Reveals Principles of Chromatin Looping. *Cell*, **159**(7): 1665–1680.
- [10] ENCODE (2012) An integrated encyclopedia of DNA elements in the human genome. *Nature*, **489**(7414): 57–74.
- [11] Boyle AP, Araya CL, Brdlik C, Cayting P, Cheng C, Cheng Y, Gardner K, Hillier LW, Janette J, *et al.* (2014) Comparative analysis of regulatory information and circuits across distant species. *Nature*, **512**(7515): 453–456.
- [12] Zhang Y, Liu T, Meyer Ca, Eeckhoutte J, Johnson DS, Bernstein BE, Nusbaum C, Myers RM, Brown M, *et al.* (2008) Model-based analysis of ChIP-Seq (MACS). *Genome biology*, **9**(9): R137.
- [13] Suzuki R, Shimodaira H (2006) Pvcust: an R package for assessing the uncertainty in hierarchical clustering. *Bioinformatics (Oxford, England)*, **22**(12): 1540–2.
- [14] Breiman L (2001) Random Forests. *Machine learning*, **45**(1): 5–32.
- [15] Liaw A, Wiener M (2002) Classification and Regression by randomForest. *R News*, **2**(December): 18–22.
- [16] Svetnik V, Liaw A, Tong C, Culberson JC, Sheridan RP, Feuston BP (2003) Random forest: a classification and regression tool for compound classification and QSAR modeling. *Journal of chemical information and computer sciences*, **43**(6): 1947–58.
- [17] Cutler DR, Edwards TC, Beard KH, Cutler A, Hess KT, Gibson J, Lawler JJ (2007) Random forests for classification in ecology. *Ecology*, **88**(11): 2783–92.
- [18] Díaz-Uriarte R, Alvarez de Andrés S (2006) Gene selection and classification of microarray data using random forest. *BMC bioinformatics*, **7**: 3.

- [19] Dasgupta A, Sun YV, König IR, Bailey-Wilson JE, Malley JD (2011) Brief review of regression-based and machine learning methods in genetic epidemiology: the Genetic Analysis Workshop 17 experience. *Genetic epidemiology*, **35** Suppl 1(Suppl 1): S5–11.
- [20] Breiman L (2001) Statistical Modeling: The Two Cultures. *Statistical Science*, **16**(3): 199–231.
- [21] Hastie T, Tibshirani R, Friedman J (2009) *Elements of Statistical Learning: Data Mining, Inference, and Prediction*. Springer, 2 edition. ISBN 978-0-387-84858-7.
- [22] Tobias RD (1995) An Introduction to Partial Least Squares Regression. *Proc. Ann. SAS Users Group Int. Conf. 20th*, pp. 1250–1257.
- [23] Friedman J, Hastie T, Tibshirani R (2008) Sparse inverse covariance estimation with the graphical lasso. *Biostatistics (Oxford, England)*, **9**(3): 432–41.
- [24] Mazumder R, Hastie T (2012) The graphical lasso: New insights and alternatives. *Electronic Journal of Statistics*, pp. 1–21.
- [25] Ernst J, Kheradpour P, Mikkelsen TS, Shores N, Ward LD, Epstein CB, Zhang X, Wang L, Issner R, *et al.* (2011) Mapping and analysis of chromatin state dynamics in nine human cell types. *Nature*, **473**(7345): 43–9.
- [26] Hoffman MM, Buske OJ, Wang J, Weng Z, Bilmes Ja, Noble WS (2012) Un-supervised pattern discovery in human chromatin structure through genomic segmentation. *Nature Methods*, **9**(5): 473–476.
- [27] Hoffman MM, Ernst J, Wilder SP, Kundaje A, Harris RS, Libbrecht M, Giardine B, Ellenbogen PM, Bilmes Ja, *et al.* (2013) Integrative annotation of chromatin elements from ENCODE data. *Nucleic acids research*, **41**(2): 827–41.
- [28] Furey TS (2003) Integration of the cytogenetic map with the draft human genome sequence. *Human Molecular Genetics*, **12**(9): 1037–1044.
- [29] Boyle S, Gilchrist S, Bridger JM, Mahy NL, Ellis Ja, Bickmore Wa (2001) The spatial organization of human chromosomes within the nuclei of normal and emerin-mutant cells. *Human molecular genetics*, **10**(3): 211–9.
- [30] Chambers EV, Bickmore Wa, Sempile CA (2013) Divergence of mammalian higher order chromatin structure is associated with developmental loci. *PLoS computational biology*, **9**(4): e1003017.
- [31] de Wit E, Bouwman BaM, Zhu Y, Klous P, Splinter E, Verstegen MJaM, Krijger PHL, Festuccia N, Nora EP, *et al.* (2013) The pluripotent genome in three dimensions is shaped around pluripotency factors. *Nature*, pp. 1–7.
- [32] Tanabe H, Müller S, Neusser M, von Hase J, Calcagno E, Cremer M, Solovei I, Cremer C, Cremer T (2002) Evolutionary conservation of chromosome territory arrangements in cell nuclei from higher primates. *Proceedings of the National Academy of Sciences of the United States of America*, **99**(7): 4424–9.
- [33] Ashburner M, Ball Ca, Blake Ja, Botstein D, Butler H, Cherry JM, Davis aP, Dolinski K, Dwight SS, *et al.* (2000) Gene ontology: tool for the unification of biology. The Gene Ontology Consortium. *Nature genetics*, **25**(1): 25–29.
- [34] Huang BDW, Lempicki R (2008) Systematic and integrative analysis of large gene lists using DAVID bioinformatics resources. *Nature protocols*, (301): 1–43.